Applied Magnetic Resonance (2020) 51:1103–1115
https://doi.org/10.1007/s00723-020-01239-5

Applied
Magnetic Resonance

REVIEW

Zero-Field Splitting Parameters of Hemin Investigated by High-Frequency and High-Pressure Electron Paramagnetic Resonance Spectroscopy

Eiji Ohmichi[1] · Tsubasa Okamoto[1] · Takahiro Sakurai[2] · Hideyuki Takahashi[3] · Susumu Okubo[3] · Hitoshi Ohta[3]

Received: 6 July 2020 / Revised: 24 July 2020 / Published online: 30 August 2020

Abstract

We systematically studied the zero-field splitting (ZFS) parameters of Fe(III) protoporphyrin IX chloride, or hemin, using the terahertz electron paramagnetic resonance (EPR) spectroscopy technique at ambient and high pressures. Although hemin is known as a model substance of hemoproteins, the pressure effect on the electronic structure has not yet been explored owing to the large ZFS. In this study, high-field and high-frequency EPR measurements were carried out in the frequency range up to 700 GHz and at hydrostatic pressures up to 2 GPa. At ambient pressure, multiple EPR branches were clearly observed, and the axial and rhombic components of ZFS were determined as $D = 6.90 \pm 0.01$ cm^{-1} and $E = 0.055 \pm 0.005$ cm^{-1}, respectively. Upon pressure application, we observed a systematic shift of the resonance field, indicating a monotonous increase of the axial component from $D = 6.9$ to 7.9 cm^{-1} at 2 GPa. The origin of this unusually large shift was discussed from a microscopic viewpoint of the electronic structure of iron under pressure.

✉ Hitoshi Ohta
hohta@kobe-u.ac.jp

Eiji Ohmichi
ohmichi@harbor.kobe-u.ac.jp

[1] Graduate School of Science, Kobe University, 1-1 Rokkodai-cho, Nada, Kobe 657-8501, Japan

[2] Research Facility Center for Science and Technology, Kobe University, 1-1 Rokkoadai-cho, Nada, Kobe 657-8501, Japan

[3] Molecular Photoscience Research Center, Kobe University, 1-1 Rokkodai-cho, Nada, Kobe 657-8501, Japan

1 Introduction

Porphyrin complexes play important roles in biochemistry [1, 2]. In particular, metalloporphyrins [3], in which a metal ion is located at the center of a porphyrin ring, are widely found in numerous proteins and enzymes, such as chlorophyll and hemoproteins. The metal ions in these complexes play functional roles in biological processes such as redox, catalysis, and electron transfer. In this sense, the electronic structures of metal ions in porphyrin complexes are crucial for understanding the functional roles of metalloproteins and metalloenzymes from a microscopic viewpoint.

It is known that hemoproteins are among the most important metalloproteins in various biological systems [4, 5]. For example, hemoglobin transports oxygen molecules in blood, and its functional center is iron protoporphyrin IX, which is also known as heme. Hemoglobin controls whether the oxygen molecule is captured or released at the iron site, depending on subtle differences in the environment. During this process, the molecular structure of heme changes accordingly; thus, the microscopic study of the electronic structure of heme, especially around an iron atom, is very important [6, 7].

Because hemin, i.e., iron(III) protoporphyrin IX chloride [3], has the same geometric structure as heme, this molecule is one of the model substances of hemoproteins (Fig. 1a). The Fe^{3+} ion located at the center of protoporphyrin IX is coordinated with four nitrogen atoms and one chlorine atom [8]. In the case of free $Fe^{3+}(3d^5)$, the ground state is a sextet ($S = 5/2, L = 0$), but for hemin, the zero-field degeneracy of the three Kramers doublets of $S = 5/2 (S_z = \pm 1/2, \pm 3/2, \pm 5/2)$ is removed by the effect of zero-field splitting (ZFS), which yields the magnetic anisotropy of the system. In the case of $S \geq 1$, ZFS is described by the following spin Hamiltonian:

$$H = DS_z^2 + E(S_x^2 - S_y^2), \tag{1}$$

where the z-axis corresponds to the direction normal to the heme plane, and the parameters D and E represent the axial and rhombic components of ZFS, respectively. Therefore, D and E primarily determine the electronic structure and magnetic anisotropy of the spin system. Thus, precise determination of these parameters is fundamentally important for the elucidation of the electronic structure and functionality of these molecules.

It should also be noted that in metalloproteins and metalloenzymes, the pressure strongly affects not only the conformation but also the active sites or metal ions [9–11] through the pressure-induced structural changes. Therefore, the effects of a high pressure on the local electronic structure of metal-ion complexes are of particular interest. However, such pressure effects on functional centers have been studied only indirectly via optical spectroscopy [12, 13] and NMR [14, 15]. On the other hand, EPR has a unique advantage in that it permits the electronic structures of metal ions to be studied selectively and directly with a high spectral resolution at the ambient pressure [16–18]. However, no high-pressure EPR studies probing the active site of hemoproteins have been reported. This is attributed to the fact that iron-porphyrin complexes generally have large ZFS parameters, necessitating

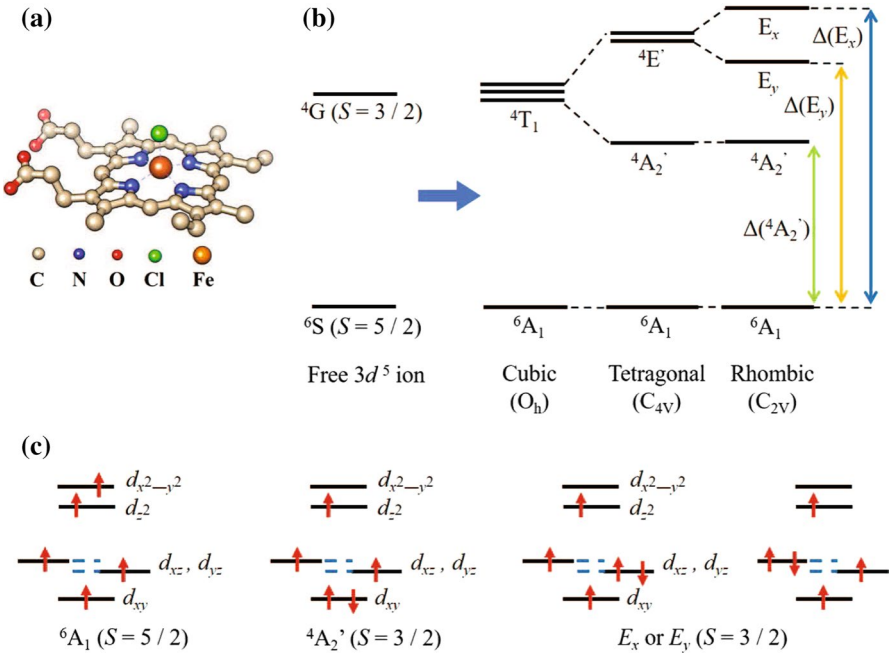

Fig. 1 **a** Three-dimensional molecular structure of hemin. **b** Multiplet energy states for the $3d^5$ system. In the case of a free ion, the ^6S and ^4G states are the lowest and second-lowest multiplets. In the presence of a ligand field, as the symmetry is reduced, the multiplet energy levels are split. The energy differences between the ground and excited states are indicated by three arrows. **c** Spin configurations of the $^6A_1$ and $^4A_2'$ and E_x or E_y ($4E'$ in the tetragonal symmetry) multiplet energy states

high-frequency EPR spectroscopy under pressure. Currently, such broadband EPR techniques under pressure are very limited [19–24]; thus, the pressure dependence of the ZFS parameter has hardly been discussed.

In this review, we show high-frequency and high-field EPR (HFEPR) results of hemin—a model substance of hemoproteins—at ambient and applied pressures using specially developed pressure cells [25–28]. We report the systematic pressure dependence of the ZFS parameter at pressures up to 2.0 GPa, in which a monotonous increase of the axial ZFS parameter upon pressure application was clearly observed [29].

2 The Electronic Structure of Hemin

First, we will briefly discuss the origins of the ZFS parameters. When we consider $3d^5$ electrons for the free Fe^{3+} ion, the ground state is in a sextet ^6S ($S = 5/2$, $L = 0$) state, as shown in Fig. 1b. In a weak ligand field, the lowest energy corresponds to a sextet $^6A_1$ ($S = 5/2$) state. Because the $^6A_1$ state possesses spatially high symmetry, a mixing between the ground state $^6A_1$ and the excited states is

needed to account for the ZFS parameters. The spin–orbit coupling is known to be a dominant source of ZFS parameters in transition metal complexes; it mixes the $^6A_1$ state with the excited states.

Figure 1b shows the excited states coupled with the $^6A_1$ state by the spin–orbit coupling. In cubic symmetry, the $^4T_1$ state is the lowest excited state, which corresponds to the $S = 3/2$ state. In tetragonal symmetry, the $^4T_1$ state is split into $^4E'$ and $^4A_2'$ states, where the $^4A_2'$ state is lower than the $^4E'$ state due to the C_{4v} symmetry of hemin. When the symmetry is lowered to rhombic symmetry, the $^4E'$ state is further split into E_x and E_y states.

Here, we define the energy difference between the $^6A_1$ state and the $^4A_2'$, E_x, or E_y state as $\Delta(^4A_2')$, $\Delta(E_x)$, or $\Delta(E_y)$, respectively. Then, the ZFS parameters D and E are given as follows:

$$D = \frac{\zeta^2}{10}\left[\frac{2}{\Delta(^4A_2')} - \left(\frac{1}{\Delta(E_x)} + \frac{1}{\Delta(E_y)}\right)\right], \tag{2}$$

$$E = \frac{\zeta^2}{10}\left[\frac{1}{\Delta(E_x)} - \frac{1}{\Delta(E_y)}\right], \tag{3}$$

where ζ is a spin–orbit interaction constant. From this equation, the E term becomes zero in tetragonal symmetry but nonzero in rhombic symmetry.

There have been numerous studies on the axial ZFS parameter of hemin, D, by HFEPR [16–18, 30–35], Mössbauer spectroscopy [36], magnetic circular dichroism (MCD) [37], far infrared (FIR) spectroscopy [38, 39], and inelastic neutron scattering (INS) [40, 41]. For example, the ZFS parameters of high-spin ferric complexes were obtained by FIR spectroscopy [38, 39], frequency-domain EPR [18, 33, 42], and INS [40, 41]. The axial component was large ($D \simeq 6.9$ cm^{-1}) compared with those of other metalloporphyrins. From the microscopic perspective, however, the origins of the ZFS parameters are not very well understood, and even the correlation between the ZFS parameters and the molecular geometric structure is not clear. Indeed, a simple ligand field theory often fails to predict proper values and even the signs of the ZFS parameters.

Recently, several groups have developed techniques to calculate the ZFS parameters on the basis of computational quantum chemical calculation [40, 43–47]. For example, the ZFS parameters of the [Fe(TPP)]X (X = F, Cl, Br, I) series [40]) were obtained by ab initio calculation. The results could explain the trend in D values, but the calculated D values were smaller than the experimentally determined D values by several factors. It is noted that high-spin ferric complexes such as [Fe(TPP)]X exhibit unusually large D values, on the order of 1–10 cm^{-1} [48, 49]), compared to other transition metal complexes (usually ~ 0.1cm^{-1}) [50]), thus making quantitative calculation very difficult. Moreover, the rhombic component E of metalloporphyrin is much smaller than D in many cases, and greater accuracy is required in the calculation.

3 Experimental Setup

3.1 HFEPR Measurement at Ambient Pressure

Powder-like hemin was purchased from Sigma Aldrich (Product No. 51280) and used as received. HFEPR measurements of hemin powder samples were performed using a field-swept transmission-type setup [51, 52]. Gunn oscillators and backward-traveling wave oscillators were used as a light source. They covered wide frequency ranges of 80–160 and 200–700 GHz, respectively. All measurements were performed at 4.2 K in this study. Pulsed magnetic fields up to 16 T were generated using a capacitor bank. To calibrate the absolute field value, an EPR standard sample, 2-diphenyl-1-picrylhydrazyl (DPPH) was used as a field marker. The field homogeneity was typically 10^{-4} within 1 mm from the field center.

3.2 HFEPR Measurement at Applied Pressures

In HFEPR measurements under applied pressure, a specially designed pressure cell [25–28] was used. A piston and a bottom backup made of alumina ceramic were employed, along with a top backup made of zirconia-based ceramic. The alumina ceramic had inferior toughness compared to the zirconia-based one but had higher transparency over the entire frequency region covered in this study. This combination allowed us to perform EPR measurements in a wide frequency range of 50–700 GHz at a maximum hydrostatic pressure of 2 GPa. Daphne 7373 oil (Idemitsu Kosan Co. Ltd.) was used as a pressure medium and was encapsulated with a sample in a Teflon capsule. The low-temperature pressure value was calibrated in advance using the pressure dependence of the superconducting transition temperature of tin. An electromagnetic wave was introduced from the top of the pressure cell into the cell body and the transmitted intensity was detected by an InSb bolometer placed at the bottom of the cryostat.

The spin sensitivity of our high-pressure EPR system was typically 10^{13} spins/Gauss. This sensitivity corresponds to a detectable sample quantity of 1.6×10^{-10} mol in the case of an EPR linewidth of 1 mT.

4 Results

4.1 HFEPR of Hemin at Ambient Pressure

Figure 2 shows the HFEPR spectra at ambient pressure at several frequencies (682, 441, 363, 287, and 105 GHz). For 105 GHz, we observed an asymmetric broad absorption characteristic of the heme structure. The effective g-values ranged from $g_{\mathrm{eff}} =$ 2–6, which is in good agreement with previous results [53]. It should be noted that g_{eff} indicates apparent g-values determined from the resonance field alone under low-field conditions. The $g_{\mathrm{eff}} = 6$ signal (usually called $g_{\mathrm{eff}}^{\mathrm{perp}}$) corresponded to the case where

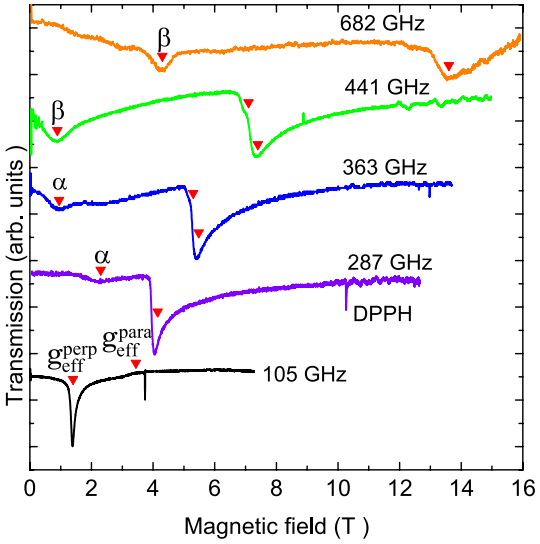

Fig. 2 Raw data of HFEPR spectra of hemin at selected frequencies. Spike-like signals near 4 and 10 T for 105 and 287 GHz, respectively, are attributed to the EPR signal of DPPH. Solid triangles indicate characteristic positions of the observed HFEPR signals

an external magnetic field was applied perpendicular to the heme normal, whereas the $g_{\mathrm{eff}} = 2$ signal (usually called $g_{\mathrm{eff}}^{\mathrm{para}}$) corresponded to the case where a magnetic field was applied parallel to the heme normal.

It is noted that an additional absorption line (assigned as the "α" branch in this paper) appeared in the lower side of the $g_{\mathrm{eff}}^{\mathrm{perp}}$ branch for 363 and 287 GHz. It was found that the resonance field of this new branch decreased as the frequency increased, and became almost zero near 400 GHz. For 441 GHz, another EPR signal (the "β" branch) was observed at approximately 1 T. This branch shifted to the higher-field region as the frequency increased, in contrast to the α branch, and was observed at 4 T for 682 GHz. In the previous EPR study [42], the $g_{\mathrm{eff}}^{\mathrm{perp}}$ and β branches were reported, but the α branch was not observed.

Looking carefully at the EPR signal of the $g_{\mathrm{eff}}^{\mathrm{perp}}$ branch for 441 GHz, a splitting of the absorption was clearly resolved. We observed similar peak splitting at different frequencies between 300 and 500 GHz. This splitting of the $g_{\mathrm{eff}}^{\mathrm{perp}}$ signal is direct evidence of the existence of an $|E|$ value, indicating non-zero magnetic anisotropy in the heme plane.

Figure 3a shows the relationships between the electromagnetic-wave frequencies and the resonance fields of all the EPR branches we observed, together with the simulation curves. We also calculated the resonance field to reproduce the experimentally observed EPR absorptions by numerical diagonalization of a spin Hamiltonian:

$$H = DS_z^2 + E(S_x^2 - S_y^2) + \mu_{\mathrm{B}} \boldsymbol{B} \cdot \boldsymbol{g} \cdot \boldsymbol{S}, \tag{4}$$

where g is the g-tensor, μ_B is the Bohr magneton, and B is the external magnetic field. In this calculation, intermolecular interactions such as exchange and dipolar interactions were not directly taken into account, because the estimated exchange interaction was very small ($J \sim 0.1\ \mathrm{cm}^{-1}$) [54] compared to the Zeeman term. The

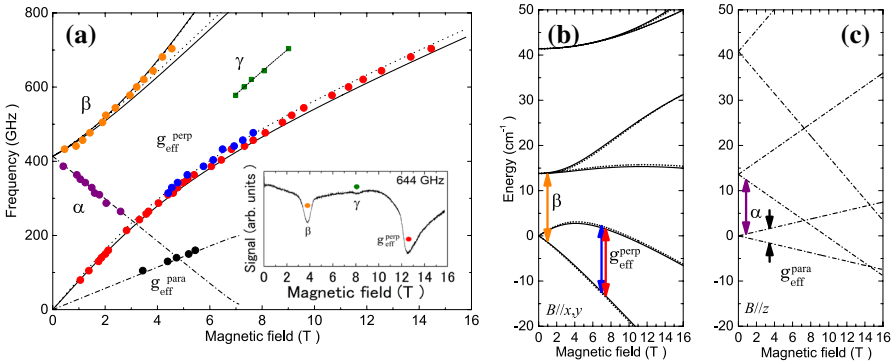

Fig. 3 **a** Electromagnetic-wave frequency versus resonance field derived from the observed EPR spectra, together with simulated curves, taking into account the ZFS parameters. Assignment of the branches is given in the text. The inset shows the magnified EPR data for 644 GHz, in which an additional weak absorption (the γ branch) was observed. **b** The calculated energy levels of hemin for $B \parallel x$, y, and vertical arrows indicate the corresponding EPR transitions for the field-swept data at 441 GHz. Curves for $B \parallel x$ and y are almost overlapped and cannot be resolved in this scale. **c** The calculated energy levels of hemin for $B \parallel z$. Purple (α) and black ($g_{\mathrm{eff}}^{\mathrm{para}}$) arrows indicate the corresponding EPR transitions for the field-swept data at 363 and 105 GHz, respectively

dipolar interaction was even smaller, and could be negligible. The effect of the exchange interaction was partly taken as the linewidth in the EPR simulation.

The solid, dotted, and dashed lines correspond to cases where an external magnetic field is applied along the x-, y-, and z-axes, respectively. In the comparison between the data and simulation, the spin Hamiltonian parameters were precisely obtained as g_x, $g_y = 1.93, g_z = 2.05, D = 6.90 \pm 0.01\mathrm{cm}^{-1}$, and $E = 0.0055 \pm 0.005\ \mathrm{cm}^{-1}$ [55], where g_x, g_y, and g_z are the intrinsic g-values for $B\|$ x, y, and z, respectively. With these parameters, all the branches were well reproduced, as shown in Fig. 3a.

For the $g_{\mathrm{eff}}^{\mathrm{perp}}$ signal, due to the existence of a small E term, two EPR transitions corresponding to $B \parallel x$ and y were visible, as shown in Fig. 3a. Further, the α branch corresponds to the EPR transition from the second to the third lowest energy state for $B \parallel z$, as shown in Fig. 3c. The β signal corresponds to the EPR transition from the lowest to the fourth lowest energy state in Fig. 3b. The $g_{\mathrm{eff}}^{\mathrm{perp}}$ branch exhibited an upward curvature. Below 300 GHz, the peak splitting was not observed, probably due to insufficient spectral resolution. Indeed, the peak splitting was not found in the numerical simulation of the EPR spectrum for 287 GHz because of the inherent broad EPR linewidth. Splitting of the $g_{\mathrm{eff}}^{\mathrm{perp}}$ branch was also not observed at frequencies beyond 500 GHz. According to a multi-frequency EPR study of myoglobin [16], EPR signals corresponding to the $g_{\mathrm{eff}}^{\mathrm{perp}}$ branch became steeply broad beyond a certain frequency due to an additional relaxation process, i.e., the Orbach process, in the high-frequency region. A similar mechanism might cause the spectral broadening of the $g_{\mathrm{eff}}^{\mathrm{perp}}$ branch in the high-frequency region.

As shown in the inset of Fig. 3a, we also observed an additional EPR signal at around 8 T for 644 GHz, though the absorption was rather weak. This signal

(denoted as the "γ" branch) was located between the β and $g_{\mathrm{eff}}^{\mathrm{perp}}$ branches, but the origin was unclear.

4.2 HFEPR of Hemin at Applied Pressures

Figure 4 shows HFEPR spectra of the hemin powder sample obtained at pressures of $P = 0, 1.00$, and 1.96 GPa. All the data were acquired for the same sample, and we confirmed that pressure-induced changes of the EPR spectra were reversible with a pressurization cycle. In this setup, the splitting of the $g_{\mathrm{eff}}^{\mathrm{perp}}$ signal was not observed at ambient pressure. An inhomogeneously distributed strain induced by the frozen pressure medium may cause additional spectral broadening. A multi-peak structure, surrounded by a dotted line, was observed near $g = 2$ for all pressure values. The origin was attributed to magnetic impurities contained in the pressure cell itself, which makes detailed analysis of the $g_{\mathrm{eff}}^{\mathrm{para}}$ difficult in the high-pressure setup.

Figure 5a shows a frequency-field diagram of three EPR branches for all pressure values. At frequencies below 350 GHz, the $g_{\mathrm{eff}}^{\mathrm{perp}}$ signals showed little pressure dependence, but above 350 Hz, they shifted slightly to the lower-field side as the pressure increased. For this reason, a pressure-induced shift of the resonance field in hemin using conventional EPR techniques has not been observed. In addition to $g_{\mathrm{eff}}^{\mathrm{perp}}$, the α branch was shifted to the higher-field side. The relationship between the frequency and the resonance field was well fitted by a straight line at all pressures, but the slope varied slightly under pressure, as discussed later. On the other hand, the β branch was shifted to the lower-field side as the pressure increased. Thus, the intersection of the α and β branches extrapolated to the zero field was shifted upward. This result clearly indicates an increase in the axial ZFS parameter D of hemin upon pressure application. For the β branch, a large pressure effect was found near the zero field, but it became small as the frequency increased, because the effect of the ZFS parameter D decreased within the high-magnetic-field limit

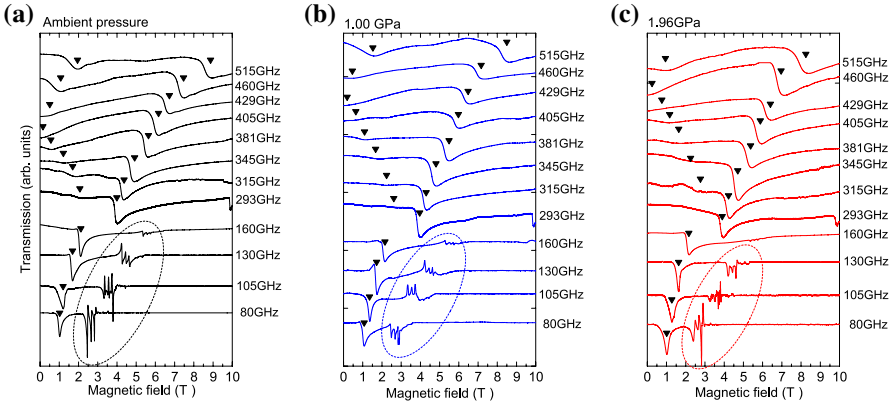

Fig. 4 (a)–(c) Multi-frequency EPR data obtained at 4.2 K for $P = 0$, 1.00 and 1.96 GPa, respectively. The data are vertically shifted for clarity. Solid triangles indicate positions of the EPR absorption. EPR signals surrounded by dotted lines originated from impurities contained in the pressure cell

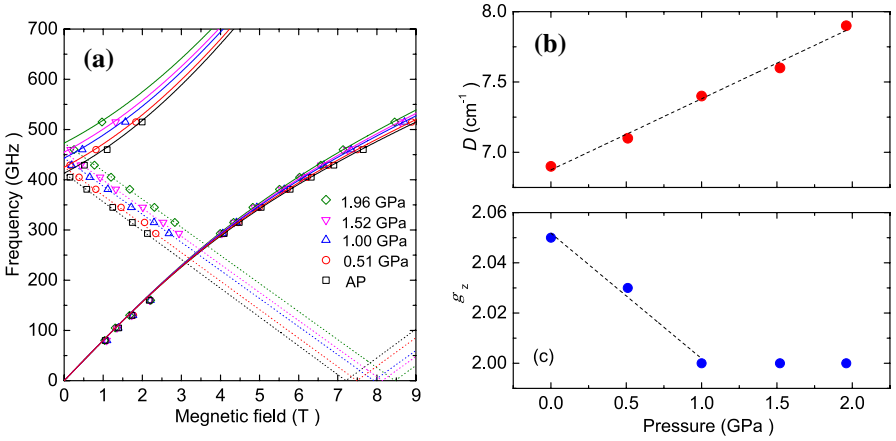

Fig. 5 **a** Electromagnetic-field frequency–resonance field diagram for all pressure values. Simulation curves (solid and dotted lines) are shown together. The pressure dependences of **b** D and **c** the intrinsic g_z are shown. Dotted straight lines are the fit result to the respective data

($D << g\mu_B B$). This trend is indicated by the simulation curves of the β branch in Fig. 5a, where all curves tend to merge together in the high-field region.

Figure 5b, c show the pressure dependence of the D term and the intrinsic g_z. The contribution of the E term was neglected in this study because of its small value compared with D ($E/D < 0.01$). Once the D values were determined, g_x and g_y were estimated to reproduce the experimentally observed $g_{\mathrm{eff}}^{\mathrm{perp}}$ signals. In addition, the g_z values were estimated from the slope of the α branch. These analyses revealed that the D value increased substantially—from 6.9 to 7.9 cm^{-1}—upon pressure application to 2 GPa. The slope of the change, obtained by a linear fitting, was 0.506 cm^{-1}/GPa. This anomalously large shift was observed for the first time using our HFEPR spectroscopy technique under pressure. It was also found that the intrinsic g_z first decreased from 2.06 to 2.00 linearly upon pressure application to 1 GPa, and then became constant up to 2 GPa. It was difficult to precisely estimate small changes in the intrinsic g_x and g_y values, owing to the broad EPR spectra, and thus previously estimated values ($g_x = g_y = 1.93$) were used for all the simulation curves.

5 Discussion

The effect of pressure on the electronic structures of iron-porphyrin complexes is not well understood. One reason for this is that these compounds have large ZFS values exceeding the energy scale of X-band EPR spectrometers, and another reason is that $g_{\mathrm{eff}}^{\mathrm{perp}}$ and $g_{\mathrm{eff}}^{\mathrm{para}}$ signals, which are usually discussed in the context of X-band experiments, exhibit little frequency dependence below 350 GHz upon application of pressure, as shown in Figs. 4 and 5. Therefore, a high-pressure EPR spectroscopy technique is needed to investigate the pressure-induced changes in the electronic structures of these complexes.

Upon the application of pressure, the crystal structure is compressed, but the compressibility is generally not uniform, because of the anisotropic nature of the molecular structure. For hemin, a porphyrin ring is composed of covalent bonds of carbon atoms and is rather rigid within the plane. Therefore, it is easier to compress the molecular structure normal to the plane, and the bond length between iron and chlorine is thought to be more sensitive than those between iron and nitrogen to the applied pressure. This anisotropic behavior was also observed in high-pressure vibrational studies of hemoproteins [12, 56, 57], where the skeletal modes of heme were slightly changed, while the axial ligands of heme were more affected upon pressure application.

In this situation, it is expected that the energy level of the d_{xy} orbital changes little. On the other hand, considering that the bonding between iron and chlorine atoms is π-antibonding, reducing the iron–chlorine distance increases the energy of the d_{yz} and d_{xz} orbitals. Accordingly, the energy difference $\Delta(4E')$ increases, and the negative contribution to D decreases, according to Eq. 3. This is a qualitative explanation of the pressure-induced increase of ZFS, which is consistent with previously reported Mössbauer results obtained under pressure [36].

To study the origins of the ZFS parameter, one can systematically change either the molecular structures or the anions of the complexes. However, the interpretation of the results induced by these changes is not straightforward, owing to the complicated origin of ZFS parameters. As discussed in Ref. [40], not only the ligand field but also numerous additional parameters must be considered to determine the ZFS parameters in quantum chemical calculations, e.g., the covalency, spin–orbit coupling constant, and relativistic effect. On the other hand, pressure is another way to control the ZFS parameters that is distinct from chemical modification. Pressure is often called a clean physical parameter because it allows reversible and continuous changes while maintaining the same atoms with the same connectivity.

Previous studies on the high-pressure effects on proteins have mainly focused on conformational changes that are induced at lower pressure. For instance, NMR [58–61], X-ray [62], infrared, and Raman spectroscopy [12, 63] have been reported below 1 GPa. On the other hand, studies on the pressure effects at the active site of a metalloprotein have been limited, even though the electronic structure of metal ions plays crucial roles in protein activities. The Mössbauer effect under pressure [9–11] was reported in relation to the local environments of iron atoms, but its application is limited to iron-containing systems. In contrast, our HFEPR technique can in principle detect any type of EPR-active spin species and is expected to have more versatile applications. HFEPR techniques are very sensitive to subtle changes in the local environment—such as changes in molecular structure, valence, and motional degrees of freedom—and have been used to investigate the active sites of metalloproteins/metalloenzymes at the ambient pressure with a high spectral resolution [16–18]. Thus, our HFEPR technique provides unique opportunities to study the effects of high pressure on such protein active sites.

In metalloproteins, metal ions are often coordinated by amino-acid residues that are a part of the protein structure. Upon pressure application, conformational changes are induced, and therefore the coordination of the amino-acid residues are affected. Such ligands are more susceptible to pressure than the chlorine atom of

hemin, and more pressure-induced changes in the EPR spectra are expected for these proteins compared with model complexes. The EPR detection of ferrous iron states under pressure is also of particular interest, as most hemeproteins are active in the ferrous state. Thus, ferrous ($S = 2$) hemoproteins [64] and hemin [65] under pressure would be worth studying in the future.

6 Summary

We studied the electronic structure of hemin using a broadband high-frequency EPR spectroscopy operated under pressure and reported the pressure dependence of the ZFS parameter of hemin—a model complex of hemoproteins—in a frequency range up to 700 GHz and at pressures up to 2 GPa. Our data clearly indicate a 30% increase of the axial ZFS parameter, D, which is explained by the anisotropic compressibility of the hemin molecule.

Our analysis was based on a ligand field theory as the crystal structure under pressure was not available. We hope that this work will stimulate further high-pressure structural investigations and subsequent quantum chemical calculations under pressure. Because pressure is recognized as a continuous and reversible physical parameter for controlling the electronic structure, the effect of pressure on the ZFS parameter provides unique opportunities to elucidate the origins and nature of the ZFS compared with other approaches based on structural modifications. To date, the effects of pressure on proteins have been studied mainly from the viewpoint of conformational changes. On the other hand, due to experimental difficulties, the pressure effects on the electronic structures of metal ions in metalloproteins/metalloenzymes have not been explored, even though these ions play crucial roles in protein activities. Therefore, the application of our high-pressure HFEPR technique to metalloproteins/metalloenzymes will be tested in the near future.

Acknowledgements The authors thank Y. Kobori (Molecular Photoscience Research Center, Kobe University) for fruitful discussions. This study was partly supported by a Grant-in-Aid for Scientific Research (B) (Grant No. 26287081), by a Grant-in-Aid for Scientific Research (C) (Grant No. 26400335), by a Grant-in-Aid for Challenging Exploratory Research (Grant No. 26610104) from JSPS, and by the Asahi Glass Foundation.

References

1. L.R. Milgrom, *The Colours of Life: An Introduction to the Chemistry of Porphyrins and Related Compounds* (Oxford University Press, New York, 1997)
2. A.N. Vzorov, D.W. Dixon, J.S. Trommel, L.G. Marzilli, R.W. Compans, Antimicrob. Agents Chemother. **46**, 3917 (2002)
3. J.E. Falk, in *Porphyrins and Metalloporphyrins*, ed. by K.M. Smith (Elsevier, Amsterdam, 1975)
4. R. Davydov, B.M. Hoffman, J. Biol. Inorg. Chem. **13**, 357 (2008)
5. S. Adachi, S.-Y. Park, J.R.H. Tame, Y. Shiro, N. Shibayama, Proc. Natl. Acad. Sci. U.S.A. **100**, 7039 (2003)
6. M. Kotani, Ann. N. Y. Acad. Sci. **158**, 20 (1969)
7. Y. Harada, M. Taguchi, Y. Miyajima, T. Tokushima, Y. Horikawa, A. Chainani, Y. Shiro, Y. Senba, H. Ohashi, H. Fukuyama et al., J. Phys. Soc. Jpn. **78**, 044802 (2009)

8. D.E. Koenig, Acta Cryst. **18**, 663 (1965)
9. A.R. Champion, H.G. Drickamer, Proc. Natl. Acad. Sci. U.S.A. **58**, 876 (1967)
10. L. Silver, R.F. George, J.R. Miller, C.A. McCammon, D.J. Evans, G.J. Leigh, Inorg. Chem. **38**, 4256 (1999)
11. M. Blume, Phys. Rev. Lett. **18**, 305 (1967)
12. O. Galkin, S. Buchter, A. Tabirian, A. Schulte, Biophys. J. **73**, 2752 (1997)
13. M.C. Marden, G.H.B. Hoa, F. Stetzkowski-Marden, Biophys. J. **49**, 619 (1986)
14. I. Morishima, M. Hara, J. Am. Chem. Soc. **104**, 6833 (1982)
15. R. Kitahara, M. Kato, Y. Taniguchi, Protein Sci. **12**, 207 (2003)
16. Y. Miyajima, H. Yashiro, T. Kashiwagi, M. Hagiwara, H. Hori, J. Phys. Soc. Jpn. **73**, 280 (2004)
17. H. Hori, H. Yashiro, M. Hagiwara, J. Inorg. Biochem. **116**, 53 (2012)
18. J. Nehrkorn, B.M. Martins, K. Holldack, S. Stoll, H. Dobbek, R. Bittl, A. Schnegg, Mol. Phys. **111**, 2696 (2013)
19. H. Ohta, S. Okubo, T. Sakurai, T. Goto, K. Kirita, K. Ueda, K.Y. Uwatoko, T. Saito, M. Azuma, M. Takano, Phys. B **294–295**, 624 (2001)
20. A.V. Kornilov, P.J.M. van Bentum, J.S. Brooks, J.S. Qualls, J.A.A.J. Perenboom, V. Pudalov, Synth. Met. **103**, 2246 (1999)
21. T. Sakurai, A. Taketani, T. Tomita, S. Okubo, H. Ohta, Y. Uwatoko, Rev. Sci. Instrum. **78**, 065107 (2007)
22. T. Sakurai, M. Tomoo, S. Okubo, H. Ohta, K. Kudo, Y. Koike, J. Phys. Conf. Ser. **150**, 042171 (2009)
23. A. Prescimone, C. Morien, D. Allan, J.A. Schlueter, S.W. Tozer, J.K. Manson, S. Parsons, E.K. Brechin, Angew. Chem. Int. Ed. **51**, 7490 (2012)
24. K. Thirunavukkuarasu, S. Winter, C.C. Beedle, A.E. Kovalev, R.T. Oakley, S. Hill, Phys. Rev. B **91**, 014412 (2015)
25. K. Fujimoto, T. Sakurai, S. Okubo, H. Ohta, K. Matsubayashi, Y. Uwatoko, K. Kudo, Y. Koike, Appl. Magn. Reson. **44**, 893 (2013)
26. T. Sakurai, K. Fujimoto, R. Matsui, K. Kawasaki, S. Okubo, H. Ohta, K. Matsubayashi, Y. Uwatoko, H. Tanaka, J. Magn. Reson. **259**, 108 (2015)
27. T. Sakurai, R. Matsui, K. Kawasaki, S. Okubo, H. Ohta, Appl. Magn. Reson. **46**, 1007 (2015)
28. T. Sakurai, S. Okubo, H. Ohta, J. Magn. Reson. **280**, 3 (2017)
29. T. Okamoto, E. Ohmichi, Y. Saito, T. Sakurai, H. Ohta, J. Phys. Chem. B **122**, 6880 (2018)
30. A. Sienkiewicz, J. Krzystek, B. Vileno, G. Chatain, A.J. Kosar, A.S. Bohle, L.J. Forró, J. Am. Chem. Soc. **128**, 4534 (2006)
31. C. Duboc, T. Phoeurg, S. Zein, J. Pécaut, M.-N. Collomb, F. Neese, Inorg. Chem. **46**, 4905 (2007)
32. M. Idešicová, J. Titiš, J. Krzystek, R. Boča, Inorg. Chem. **52**, 9409 (2013)
33. G.C. Brackett, P.L. Richards, W.S. Caughey, J. Chem. Phys. **54**, 4383 (1971)
34. J.E. Bennett, J.F. Gibson, D.J.E. Ingram, Proc. R. Soc. A **240**, 67 (1957)
35. M.P. Hendrich, P.G. Debrunner, Biophys. J. **56**, 489 (1989)
36. A.J. Bearden, T.H. Moss, W.S. Caughey, C.A. Beaudreau, Proc. Natl. Acad. Sci. U.S.A. **53**, 1246 (1965)
37. F. Paulat, N. Lehnert, Inorg. Chem. **47**, 4963 (2008)
38. K. Sakai, H. Masumoto, K. Ichimura, H. Kojima, Appl. Opt. **17**, 1709 (1978)
39. H. Uenoyama, Biochim. Biophys. Acta Gen. Subj. **230**, 479 (1971)
40. S.E. Stavretis, M. Atanasov, A.A. Podlesnyak, S.C. Hunter, F. Neese, Z.-L. Xue, Inorg. Chem. **54**, 9790 (2015)
41. S.C. Hunter, A.A. Podlesnyak, Z.-L. Xue, Inorg. Chem. **53**, 1955 (2014)
42. J. Nehrkorn, J. Telser, K. Holldack, S. Stoll, A. Schnegg, J. Phys. Chem. B **119**, 13816 (2015)
43. F. Neese, E.I. Solomon, Inorg. Chem. **37**, 6568 (1998)
44. Q.-Z. Lü, Y. Lu, J.-J. Wang, Chin. J. Chem. Phys. **19**, 227 (2006)
45. F. Neese, J. Chem. Phys. **127**, 164112 (2007)
46. D. Ganyushin, F. Neese, J. Chem. Phys. **125**, 024103 (2006)
47. R. Takeda, M. Shoji, S. Yamanaka, K. Yamaguchi, Polyhedron **24**, 2238 (2005)
48. J. Krzystek, D. Smirnov, C. Schlegel, J.V. Slageren, J. Telser, A. Ozarowski, J. Magn. Reson. **213**, 158 (2011)
49. A.S. Brill, F.G. Fiamingo, D.A. Hampton, J. Inorg. Biochem. **28**, 137 (1986)
50. A. Solano-Peralta, J.P. Saucedo-Vazquez, E. Roberto, H. Herbert, E.M. Hassane, G.M. Smith, M.E. Sosa-Torres, Dalton Trans. **9**, 1668 (2009)

51. M. Motokawa, H. Ohta, N. Makita, Int. J. Infrared Millim. Waves **12**, 149 (1991)
52. S. Kimura, H. Ohta, M. Motokawa, S. Mitsudo, W.-J. Jang, M. Hasegawa, H. Takei, Int. J. Infrared Millim. Waves **17**, 833 (1996)
53. T. Yonetani, H. Schleyer, J. Biol. Chem. **242**, 3926 (1967)
54. J. Ernst, J. Subramanian, J.-H. Fuhrhop, Z. Naturforsch A. **32**, 1129 (1977)
55. T. Okamoto, E. Ohmichi, S. Okubo, H. Ohta, J. Phys. Soc. Jpn. **87**, 013702 (2018)
56. R.G. Alden, J.D. Satterlee, J. Mintrovich, I. Constantindis, M.R. Ondrias, B.I. Swanson, J. Biol. Chem. **264**, 1933 (1989)
57. C. Jung, O. Ristau, H. Schulze, S.G. Sligar, Eur. J. Biochem. **235**, 660 (1996)
58. K. Akasaka, Chem. Rev. **106**, 1814 (2006)
59. L.M. Nguyen, J. Roche, J. Magn. Reson. **277**, 179 (2017)
60. J. Jonas, L. Ballard, D. Nash, Biophys. J. **75**, 445 (1998)
61. A. Maeno, D. Sindhikara, F. Hirata, R. Otten, F.W. Dahlquist, S. Yokoyama, K. Akasaka, F.A.A. Mulder, R. Kitahara, Biophys. J. **108**, 133 (2015)
62. H. Yamada, T. Nagae, N. Watanabe, Acta Crystallogr. Sect. D: Biol. Crystallogr. **71**, 742 (2015)
63. M. Klepacka, K. Bajdor, A. Jezewski, Pol. J. Food Nutr. Sci. **48**, 275 (1998)
64. H. Hori, H. Yashiro, K. Ninomiya, M. Horitani, T. Kida, M. Hagiwara, J. Inorg. Biochem. **105**, 1596 (2011)
65. S.O. Obare, T. Ito, M.H. Balfour, G.J. Meyer, Nano Lett. **3**, 1151 (2003)